Available online at www.sciencedirect.com
ScienceDirect
Journal of Photochemistry and Photobiology A: Chemistry 193 (2008) 42–49
Journal of Photochemistry and Photobiology A:Chemistry
www.elsevier.com/locate/jphotochem

Molecular implantation using a laser-induced molecular micro-jet

Yuriy Pihosh [a,*], Masahiro Goto [a], Marat B. Gaifullin [b], Akira Kasahara [a], Masahiro Tosa [a]

[a] *Materials Reliability Centre, National Institute for Materials Science (NIMS), 1-2-1 Sengen, Tsukuba, Ibaraki 305-0047, Japan*
[b] *Superconducting Materials Center, National Institute for Materials Science (NIMS), 1-2-1 Sengen, Tsukuba, Ibaraki 305-0047, Japan*

Received 31 January 2007; received in revised form 9 May 2007; accepted 11 June 2007
Available online 14 June 2007

Abstract

Implantation of organic molecules into conductive organic or inorganic materials on the nanometre scale is one of the challenging problems in materials research that has to be solved. We have developed an advanced method of laser implantation suitable for producing organic molecular dots with sizes of a few hundred nanometres on organic and inorganic solid materials. This method involves transferring of organic molecules from a source film to a target material through a water-filled space-gap using a laser-induced molecular micro-jet. In this way, organic dots of Coumarin 6 (C6) molecules were successfully implanted into different target materials such as polymer, glass, copper, indium tin oxide (ITO), stainless steel, and so on. The shapes of the implanted dots as well as the shapes of the holes, caused by damage to the source or target films during laser irradiation, depended on whether water or air filled the space-gap between the films.

Keywords: Coumarin 6; Implantation; Molecular jet; Re-entrant micro-jet; Organic dot

1. Introduction

Recently researchers have continuously been trying to engineer smaller and smaller devices. Their aim is to develop new types of molecular devices, such as nano-molecular sensors and photonic devices, with more advanced functions, structures, etc. In particular, in order to construct surface molecular nanostructures and nano-devices, the process of self-assembly of organic molecules is considered necessary. This process plays a crucial role in the so-called "bottom-up" strategy of nanofabrication, since a self-organized molecular pattern, with its structure and its derived concomitant function controlled, could provide promising materials for construction of nano-devices. Another important route in fabricating nano-devices involves space selectivity and control of the process of fixing organic molecules onto the surface of substrates made from various kinds of materials. There are a number of well-known techniques, which can be used to prepare molecular nano-dots. For example, STM and AFM have proven to be powerful tools for addressing, analyzing and modifying self-assembled molecular structures as well as single atoms. However, when using these techniques, preparation of extended nano-patterns of molecules covering a larger area is impossible, as this would require a long time and considerable expenses.

The third method, which can be used to fix molecules onto the surface of a material, is laser molecular implantation (LMI). The first report on laser-induced implantation of organic molecules into a polymer surface [1] highlighted the fundamental aspects and possible practical application of this process. This method has attracted significant interest for its potential use in advanced technological applications, such as in demonstrating laser-induced mixing of two different chemicals in a polymer solid [2]. It would also be useful for fabricating the devices where functional organic molecules could be arranged in a spatially selective manner in or on a substrate [3]. Another possibility to make use of the laser implantation technique is to apply it for etching lithographic patterns. Such patterns could be formed from the molecules having functionality such as fluorescence [4,5] or photochromism [6]. The advantage of the LMI method over some others lies in the fact that it can be comparatively easily used in medical practice [7].

In order to reduce the achievable size of features, created by micro-patterning using laser light, several LMI techniques have been developed [8,9]. One of them, for example, is the

* Corresponding author at: Micro-Nano Materials Engineering Group, Materials Reliability Center, National Institute for Materials Science (NIMS), 1-2-1 Sengen, Tsukuba, Ibaraki 305-0047, Japan. Tel.: +81 29 859 6533; fax: +81 29 859 2501.
E-mail address: Yuriy.Pihosh@nims.go.jp (Y. Pihosh).

1010-6030/$ – see front matter © 2007 Elsevier B.V. All rights reserved.
doi:10.1016/j.jphotochem.2007.06.005

technique of ablative transfer of organic matter from a doped nano-pipette to a surface, after laser activation. Using this technique, the authors managed to obtain molecularly doped regions with dimensions of 600 nm [10,11]. However, the drawback of this technique is that, when repeating the experiment on a bigger area, the implanted dots disperse in a rather sporadic manner.

In previous works we reported on the development of another technique, which was laser ablative transfer of Coumarin 6 (C6) from a doped polymer film to an un-doped one [12,13]. The obtained implanted dot had a minimum size of about 3 μm. In that case, the quality of implantation was highly reproducible. However, we found that the size of the implanted dots depends on the distance between the source and target films, laser fluence and the shape of an ablated plume. In the case of high laser fluence the shape of the injected plume is affected by collisions of disintegrated particles, which also influence the size of an implanted dot. To eliminate that side effect, we performed experiments where the distance between the source and target films was filled with water [14,15]. It was found then that the size of the implanted molecular dots decreases to a submicron region.

Here we will describe in detail an advanced process of laser molecular implantation of molecules into different materials by generating a laser-induced molecular micro-jet (LIMMJ). This process leads to a significant reduction in the size of organic molecular dots implanted into various kinds of materials like solid polymer, glass or conductive materials, such as copper, ITO and stainless steel.

2. Experimental

Coumarin 6 dots have been produced in the molecular implantation process using a LIMMJ. The experimental setup is shown in Fig. 1. A single focused laser pulse (4 ns pulse, 440 nm wavelength, Coumarin dye pumped by an LSI-VSL-337ND-S nitrogen laser) was used to irradiate the source films (Coumarin 6/(poly-(butyl methacrylate)) (C6/PBMA) with a concentration of 4 wt%, which were prepared by dissolving the corresponding component (C6 and PBMA (Aldrich®) in monochlorobenzene (from Wako®)). First, the source film was spin coated onto a cover glass (Borosilicate glass from Matsunami®) about 170 μm thick, and then the prepared source C6/PBMA film was brought into contact with the target. The gap between them was filled with air or water. The air and the water environment will be further denoted as the *dry* and the *wet* gap, respectively. Several types of experiments at *dry* and *wet* gaps were performed at different laser intensities using various substrates, namely: PBMA film, glass, indium tin oxide coating (ITO), copper and stainless steel. The implantation area, which position was pre-determined by computer control of the X–Y stage, was observed by a conventional fluorescence microscope (Olympus, model—IX70). The size of each implanted dot was estimated by fitting the fluorescence intensity profile with a 1/*e* Gaussian distribution function. Fluorescence spectra from the source film and the target surface were observed with a spectrometer (Ocean Optics Inc., USB-2000-FLG), while the surface morphology of the targets was observed by an atomic force microscope (AFM) (JEOL, model—JSPM 5200). The implanted dots were analysed with the help of micro-Raman scattering (Horiba Ltd., model—HR 800 V).

3. Results and discussion

3.1. Implantation of C6 molecular dots and their morphology

To understand the mechanism of laser molecular implantation of organic dots through *dry* and *wet* gaps we investigated the

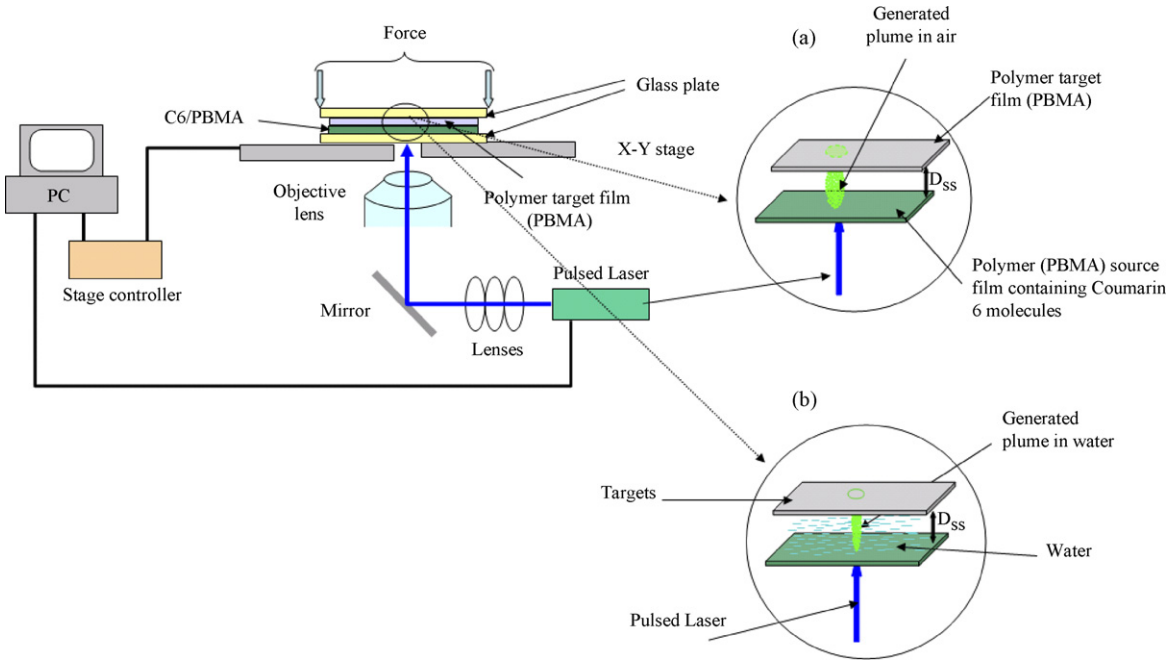

Fig. 1. Schematic illustration of the experimental setup used for laser molecular implantation of C6 molecules into PBMA poly(butyl-methacrylate) films at a *dry* interface (a): implantation of C6 molecules into cover glass, PBMA, stainless steel, copper and ITO at a *wet* interface (b).

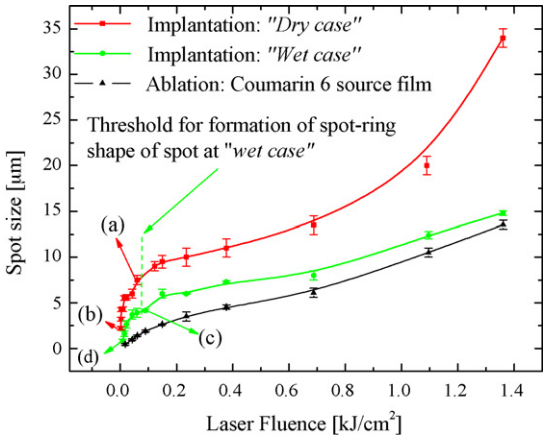

Fig. 2. Dependence of the size of the C6 spots implanted on PBMA target films, upon the laser intensity at *wet* and *dry* gaps.

relationship between the sizes of implanted C6 dots prepared under different conditions. The results of implantation of C6 dots in PBMA targets through *dry* and *wet* gaps are shown in Fig. 2, when the gap between the source and target films was less than 1 μm for the *dry* case and 2 μm for the *wet* case. Here we observed an increase in the ablation area on the source film and in the implanted dot area on the target film at both *dry* and *wet* interfaces with increasing laser fluences. From Fig. 2 it is seen that the size of the implanted dots on a PBMA target film is much bigger than that of the ablation area of the source film, when using a *dry* gap. However in the case of a *wet* gap, the size of the implanted dots and the size of the ablation area of the source film were approximately the same. Moreover, the dot size was much smaller if compared to the one in the *dry* gap case.

The size of the smallest dot for the both cases was estimated to be about 2.2 and 0.8 μm at laser fluences 2.3 and 8.8 J/cm^2 (see Fig. 2b and d), respectively. We note an interesting fact that, at laser fluence of 70 J/cm^2, a threshold appears when the shape of the dots implanted at the *wet* gap undergoes a transformation. Fig. 3 shows an optical image of the source films, fluorescence images of the implanted C6 dots on the target polymer films and the fluorescence intensity profile of the smallest dots obtained at *dry* and *wet* gaps. In the case of a *wet* gap, the implanted dots below the threshold acquire the shape (Fig. 3d) which is different from that of the dots above the threshold. The former having a donut type of shape (Fig. 3c) will be henceforth referred to as rings. In the case of the *wet* gap, we observe a phenomenon of a so-called laser-induced molecular micro-jet (LIMMJ) appearance [14]. When using the water layer, we found that it was possible to implant or fix organic molecules into different materials such as glass, ITO film, copper and stainless steel, over a much smaller area than for LMI, without the molecules getting decomposed. When using stainless steel, the molecules could not penetrate into the target material to a nanocrystal at least partly. However, the ejected dyes are at least fragmented into a molecular level, and that means that we are dealing with not laser implantation, but laser deposition.

It is necessary to add that after each experiment the source C6 film was removed from the target material, and then the target

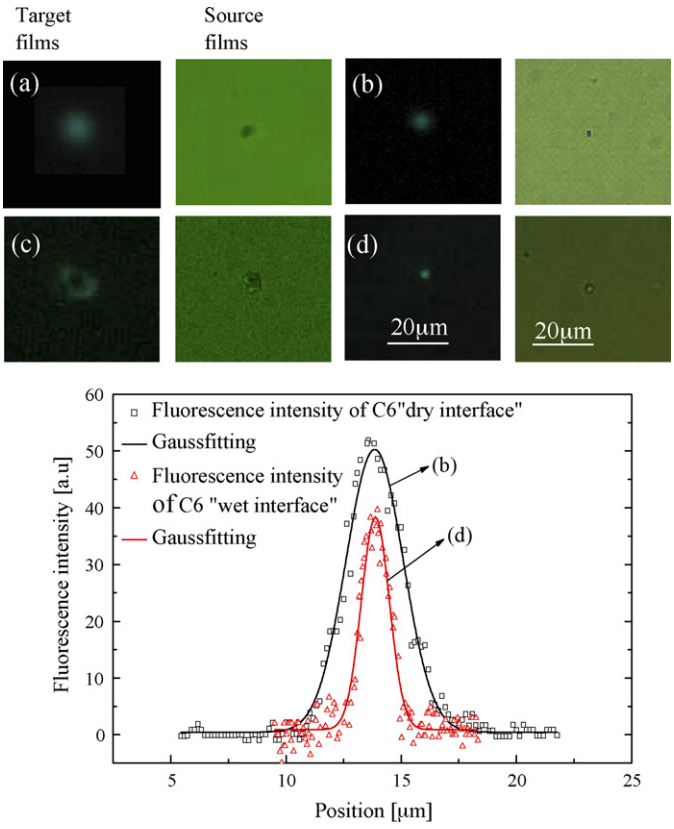

Fig. 3. Fluorescence micro-images of implanted spots on PBMA target films and microscope images of source films at *dry* (a, b) and *wet* (c, d) gaps at various laser fluences 60 J/cm^2, 2.3 J/cm^2 and 90 J/cm^2, 8 J/cm^2, respectively; and the fluorescence intensity profiles of the smallest C6 dots (the short wavelength region (<460 nm) was cut owing to a colour filter in order to avoid the excitation light for all fluorescence spectra).

was cleaned with pure water again in order to take out non-implanted organic materials. Figs. 4a and 5c show the change in the ring and dot sizes of C6 at various laser intensities. For the transparent targets (see Fig. 4a), we observed linear behaviour in the growth of the C6 dots and rings with increasing laser fluence.

We noted previously that at intermediate laser intensities there is a threshold where the shape of the implanted dots undergoes transformation to a ring type. This interesting effect was found at different laser fluence thresholds for different targets, namely: for glass at 540 J/cm^2, ITO film at 150 J/cm^2, for copper at 60 J/cm^2 and for stainless steel at 32 J/cm^2 (Figs. 4a and 5c). The minimum size of a C6 dot was achieved for all types of targets using the LIMMJ effect, and was estimated for glass as 2 μm at laser fluence of 80 J/cm^2, for ITO 0.9 μm at 60 J/cm^2, for copper 0.7 μm at 2.3 J/cm^2 and for stainless steel 0.55 μm at 8.8 J/cm^2. From Figs. 4b and 5d we can see the fluorescence spectra of the pristine source C6 film and the dots prepared on different targets at the lowest laser fluence. Also during the implantation the same spectra were observed from laser-induced fluorescence in the breakdown plasma [15]. This is a clear evidence that some of the implanted or deposited molecules did not decompose. The appearance of the second peak in Figs. 4b and 5d was never observed in laser-induced fluorescence spectra. Its intensity depends on substrate materials, and

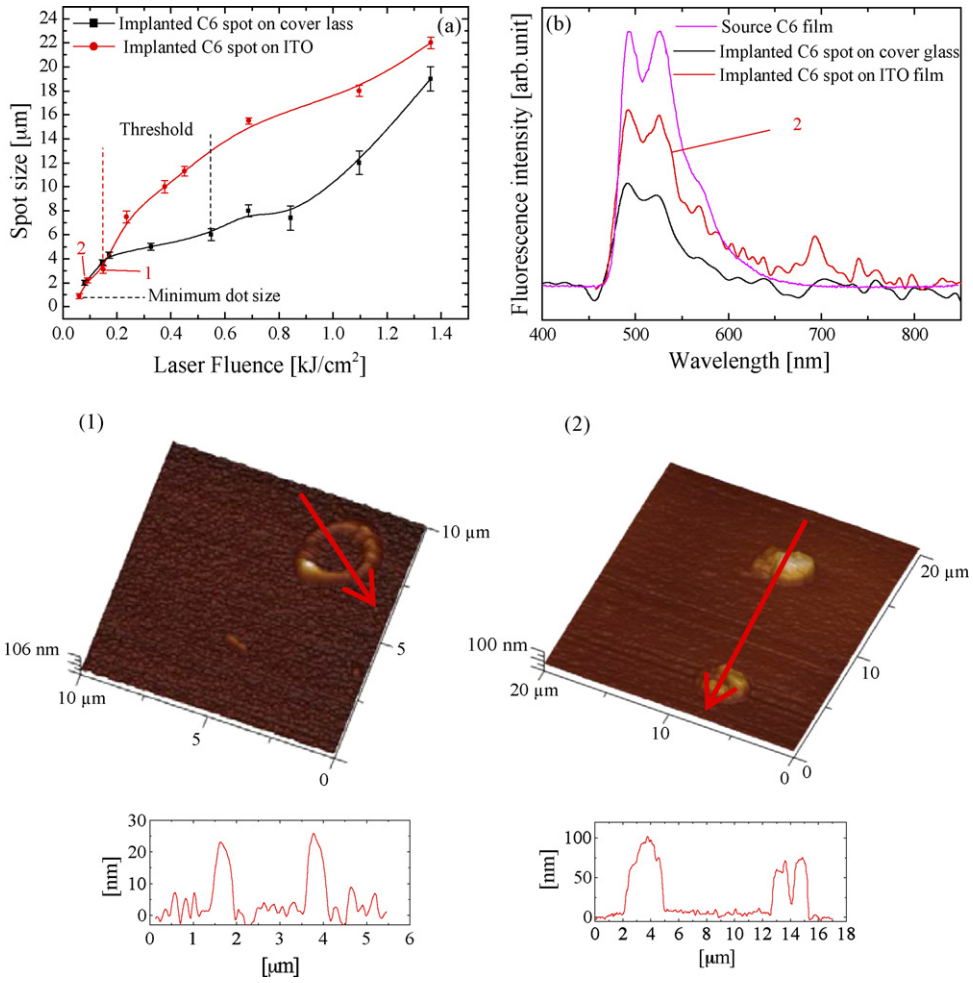

Fig. 4. Dependence of the size of an implanted spot on laser fluence (a); fluorescence spectra of a pristine source film and the dots prepared at low energy on cover glass (black line) and ITO (red line) at the *wet* gap (b); AFM images of the implanted C6 molecules into ITO surface at two various fluences: (1) at 149 J/cm^2 and (2) at 90 J/cm^2, and their cross-section profiles.

the strongest peak comes from a copper substrate. We could not see the second peak in the case of a glass substrate.

The surface morphologies of the implanted or deposited rings and dots were determined using AFM in contact mode and are shown in Figs. 4(1), (2) and 5(3)–(6) for the rings and dots prepared at high and low laser fluences. In order to detect a prepared dot, we performed AFM measurements with scanning size 25 μm × 25 μm. On finding it, we changed the size of the scanned area and pre-scanned the same dot again at high resolution. The depth of the rings and the height of the prepared dots are different and depend on the type of the target. From these figures it is clearly seen that the dot prepared at low laser fluence is implanted into different targets without etching the surface of the target, and their height was estimated to be about 100 nm for ITO, 350 nm for copper and 250 nm for stainless steel targets. Here we note that the implanted or deposited C6 dots and rings onto or into all types of targets have good adhesion and stability due to the cleaning of targets and, also, to AFM measurements. From the AFM images that were obtained from the first and the second scanning we could not see any changes in the prepared dots or rings.

3.2. Raman measurements

Fig. 6a and b show the Raman spectra (at $\lambda_{ex} = 632.89$ nm) of C6 dots implanted into copper at laser fluences of 320 and 16 J/cm^2. The observed Raman spectra occur due to surface-enhanced resonant Raman scattering (SERS). We also noticed that there was an enhanced Raman intensity and shifts of specific Raman-shifted lines, induced by the chemical interaction between a copper target and organic molecules. The spectra are in good agreement with previously published ensemble spectra [16–18]. Measurements of the Raman spectra for C6 dots implanted under the same experimental conditions, but on a glass substrate, did not give any signal. Therefore, we propose that Cu–plasmon couples to Coumarin giving a resonant absorption. It can be explained, if we consider that a metal surface is rough (in our case about 15–17 nm) on a nanometric scale, and that it contains complex electromagnetic modes. These modes modify spectroscopic properties of an absorbed molecule in a radical manner by changing the laser filed incident on the molecules. Enhanced molecular absorption might be seen for the molecules placed near the Cu-rough surface, provided that the molecu-

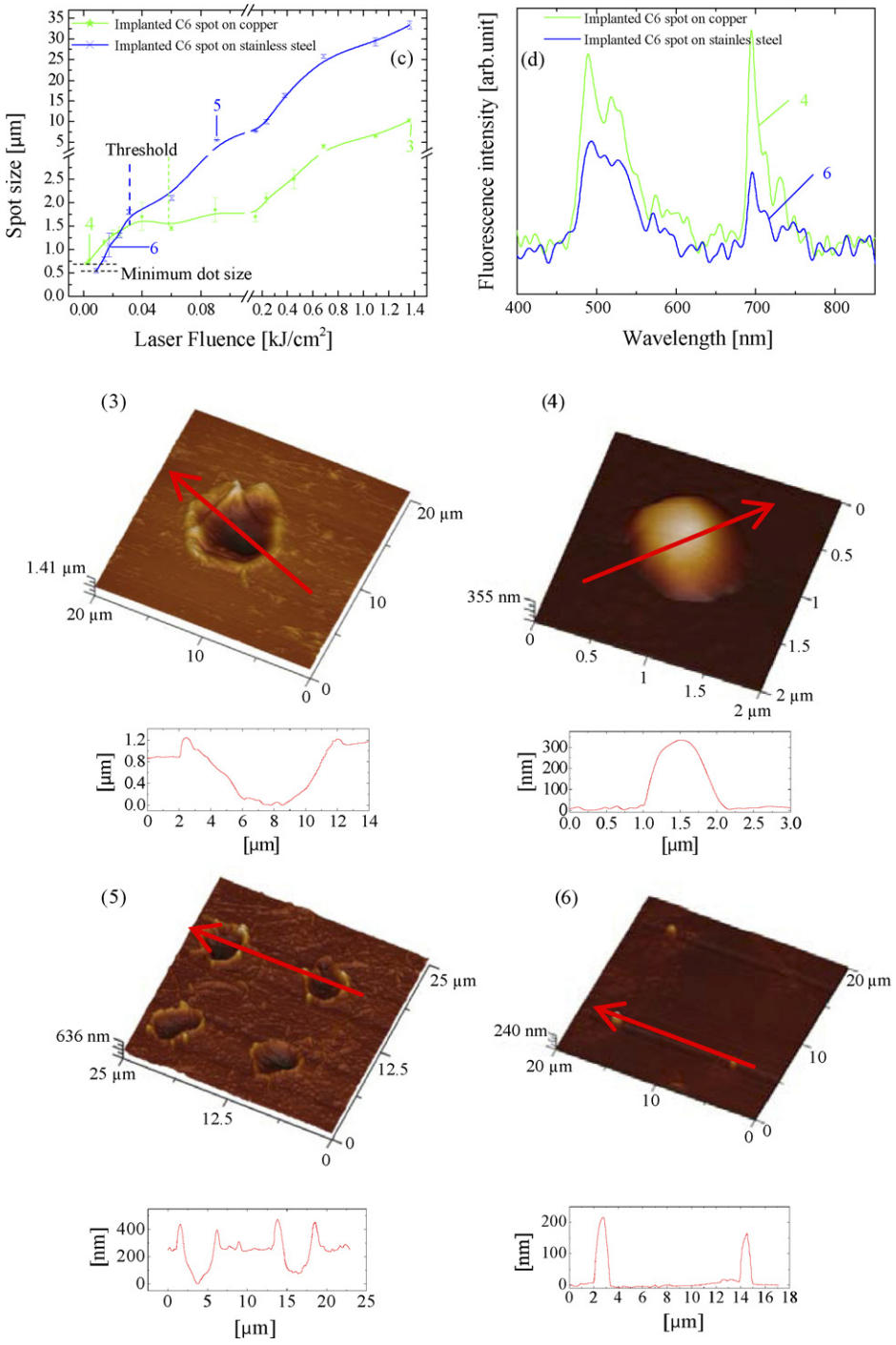

Fig. 5. Dependence of the size of an implanted spot on laser fluence (c); fluorescence spectra of the dots prepared at low energy on copper (green line) and stainless steel (blue line) at the *wet* gap (d); AFM images of the implanted and laser deposited C6 molecules at two laser fluences into copper at 1360 J/cm^2 (3) and 3.9 J/cm^2 (4); stainless steel at 90 J/cm^2 (5) and at 17 J/cm^2 (6), respectively, and their cross-section profiles.

lar absorption bands are close to the dipolar surface-plasmon frequency of the copper surface [19,20].

Several Raman-shifted lines of the C6 molecules were observed and indicated by arrows on the spectra. The peaks at 628 and 1125 cm^{-1} are assigned to the C–C–C and C–H in-plane bending vibration mode, respectively; the peak at 1250 cm^{-1} is assigned to the COH bending vibration mode; and the peaks at 1292 and 1432 cm^{-1} are assigned to the C–O–C and C–C stretching vibration mode, respectively. The peak at 1363 cm^{-1} is assigned to the *N*-phenyl vibration mode; the peak at 1478 cm^{-1} is assigned to the CH_2 bending mode (angle of H–C–H changes); and the peak at 1586 cm^{-1} is assigned to the C=C stretching vibration mode of a benzene ring. Fig. 6c and d show an optical image of a ring and a dot prepared on a copper substrate. To investigate the spatial distribution of C6 in the ring and the dot prepared on copper we used Raman peaks at 1432

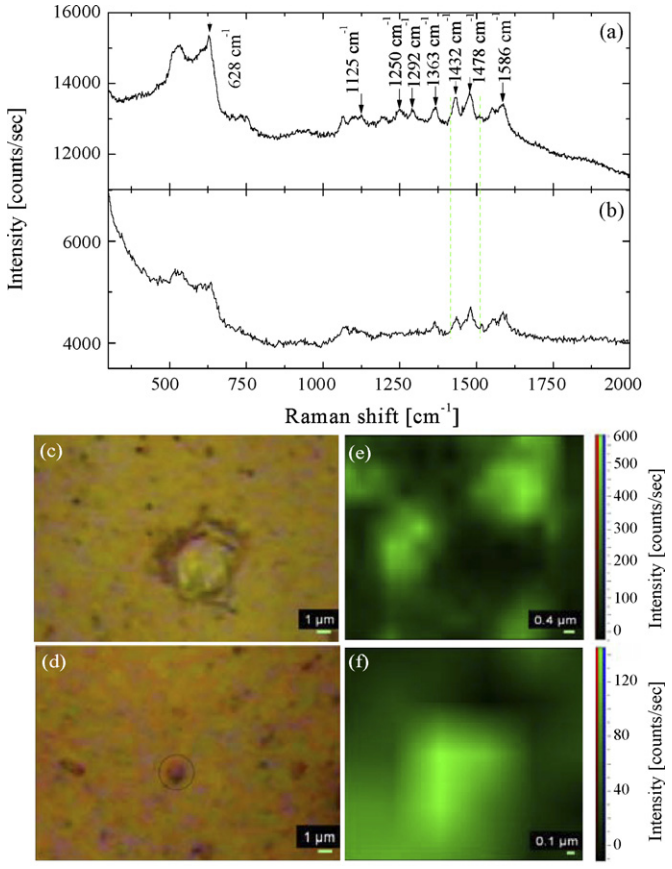

Fig. 6. Raman spectra of C6 molecules implanted into copper at two laser fluences (a, 320 J/cm^2 and b, 16 J/cm^2); optical images of prepared rings and dots (c and d) and the map of intensity of the Raman response corresponding to the position of green line in the Raman spectra.

and 1478 cm^{-1} to build a two-dimensional near-field Raman image (see Fig. 6e and f). We found that the C6 molecules are mainly localized around the hole in the ring form. The selective enhancement and the shift lines of the C6 molecules may come from the chemical interaction between them and the target.

3.3. Mechanism of implantation using a laser-induced molecular micro-jet

In the following section we will qualitatively explain the underlying mechanisms behind laser doping through a water layer in our experiments, which have been performed at high power densities ranging between 2 and 20 GW/cm^2. Under such conditions, the laser action is dominated by laser-induced breakdown of water, plasma formation, shock waves, rapid bubble growth and bubble collapse. At the present stage quantitative considerations of the real model is beyond our knowledge, because we do not have enough information about the nature of the implantation mechanism. Also, time resolved measurements of the conditions described below are necessary in order to clearly understand the mechanism of implantation when using the LIMMJ.

In order to explain the implantation process at the gap less than 2 μm filled with water, we suggest the following hypothetical mechanism as shown in Fig. 7b. Within the 4 ns laser pulse a strong electric field in focus induced multi-photonic breakdown in water and created hot plasma (at the moment t_1), which expanded, generating shock waves, and simultaneously cooled [21]. At the same time, due to light absorption (both single and multi-photonic), the temperature on the surface of the source film increased causing localized transient heating of molecules. This resulted in the explosion and further ejection of a condensed material perpendicular to the source film. Due to that process the C6 molecules could reach the target within the plasma expansion in the shock wave (at t_2, t_3). The C6 molecules were then injected into the target acquiring a form of a plume (Fig. 5(4)). At high laser fluences we observe expansion of a generated plume, which caused an effect when the shape of the dots transformed into the hole-ring type (Fig. 5(3)).

The difference in the dot size in the case of a *dry* gap could be explained if we consider the process of light absorption by the organic molecules in the source films (see Fig. 7a). When a strong nanosecond laser pulse is focused near to the source film, the hot laser plasma in the air generates a spherical shape tight shock wave compression, and due to this effect, hot dopant molecules can disperse from the source film radially in any direction of the hemisphere. Further, the dopant molecules can spread within a large area onto the target film. It is necessary to mention that at higher laser fluences even more material is ejected from the source film to the target than at low laser fluences (see Fig. 7a).

The formation of the holes and rings on copper at a *wet* gap could be examined by means of comparing the holes and the rings size when the target was introduced at different distances above the source C6 film surface at two laser fluences (see Fig. 8a and b). From this figure it can be seen that the diameter of the holes and rings increases together with increasing distance between the interfaces. This happens because the exploding front of a material has a cone shape. As a result, the diameter of the both ablated and contaminated regions increases with the distance as shown in Fig. 8. The angular spread of the C6 molecules is less than in the air because the compressibility of water is several orders of magnitude lower than that of air.

At low power densities and with a large gap between the source and target films in the case of copper and stainless steel, we suggest a two-phased process. In the first phase during the period t_1–t_3 as in Fig. 7c, a water jet formed after the absorption of a heating pulse and the vaporization of the C6 molecules from the surface. However, C6 molecules in the water jet could not reach the target from a long distance if compared to air, because of a low compressibility and turbulence in the water at this high micro-jet velocity. This is because the jet would disintegrate soon after it formed due to hydrodynamic instabilities. In the second stage, at times t_4 and t_5, the C6 molecules are captured by cavitation bubbles grown within the heated area of the plasma. The breakdown at the surface of metals usually has a lower threshold than for water and dielectrics. At a very short exposure time the size of that ring on a copper target is given by

$$D = d + 2l_{\text{th}} \quad (1)$$

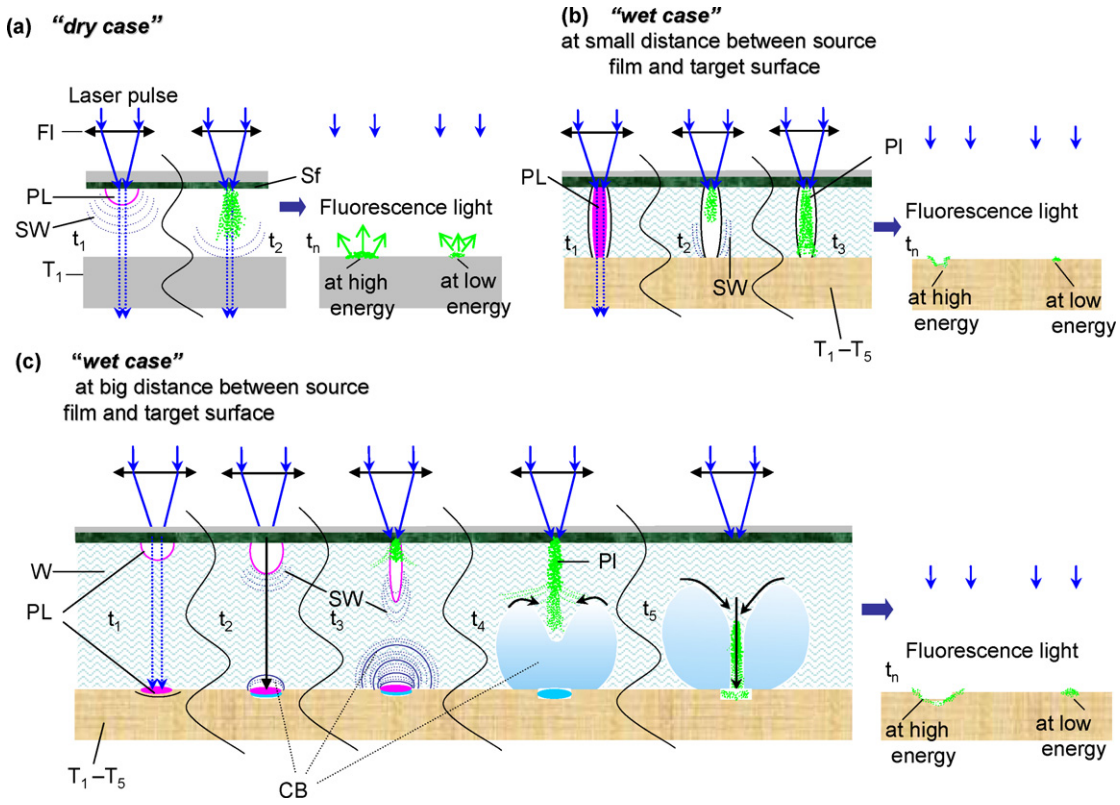

Fig. 7. Suggested mechanism of laser molecular implantation at *dry* (a) and *wet* (b) interfaces at different laser intensities on various types of substrates (Fl: focusing lens; Sf: source film; Fl: focusing lens; Pl: generated plume; PL: plasma; SW: shock wave; T: targets—T_1, PBMA; T_2, glass; T_3, ITO; T_4, copper; T_5, stainless steel; W: water; t: time; CB: cavitation bubble).

where d is the laser beam diameter, l_{th} is thermal diffusion length $l_{th} = \sqrt{\alpha\tau_p}$, where τ_p and α are laser pulse width and diffusivity coefficient of copper. In our experiment $\tau_p = 4$ ns, $l_{th} = 0.7$ μm, and the initial size of the laser spot is about 2 μm. As it is well known from fluid dynamics of liquids, an oscillating bubble is confined near to a rigid surface such as copper by the Bjerknes force at a distance of about its radius [20]. Near a rigid wall the bubble usually tends to collapse asymmetrically, forming a fast-moving re-entrant liquid jet of water. The pressure associated with the micro-jet velocity can exceed hundreds of MPa on the solid boundary [22,23]. That re-entrant micro-jet creates highly localized surface damage and causes doping of a material into a metal even from remote distances in the liquid. As seen in Fig. 8 the size of the hole in copper and the size of the C6 ring are reduced by the effect of focusing in the micro-jet with increasing distance between the interfaces. The maximum spot radius corresponds to the condition where the interface space leaves enough room for the formation of a cavitation bubble. From that we can roughly estimate the maximal diameter of a cavitation bubble. At fluence $F_2 = 0.23$ kJ/cm^2 it is about $D_{F_2} = 10$ μm. From theory [11] we know that with increasing fluence the diameter changes as follows:

$$D_{F_1} = D_{F_2}\left(\frac{F_1}{F_2}\right)^{1/3} \quad (2)$$

and is equal to 14 μm. That coincides with the peak in the spot size at fluence $F_1 = 0.68$ kJ/cm^2 on the same figure. A similar mechanism for doping exists near any rigid surface in water including transparent materials. This proves the possibility of organic molecules to be implanted into different materials by means of a laser-induced water channelled jet.

In Fig. 9 we demonstrate the possibility of space selectively fixing Coumarin 6 molecules onto a stainless steel substrate by a LIMMJ. The average size of laser deposited C6 dots was 575 ± 30 nm. As far as it is known, this is the first successful demonstration of fabricating such small C6 dots on a hard con-

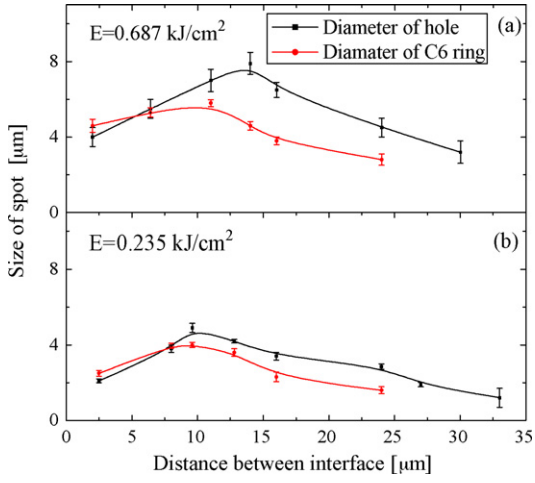

Fig. 8. Dependence of the holes and rings sizes prepared on copper with different distances between the source film and the copper target at two laser intensities.

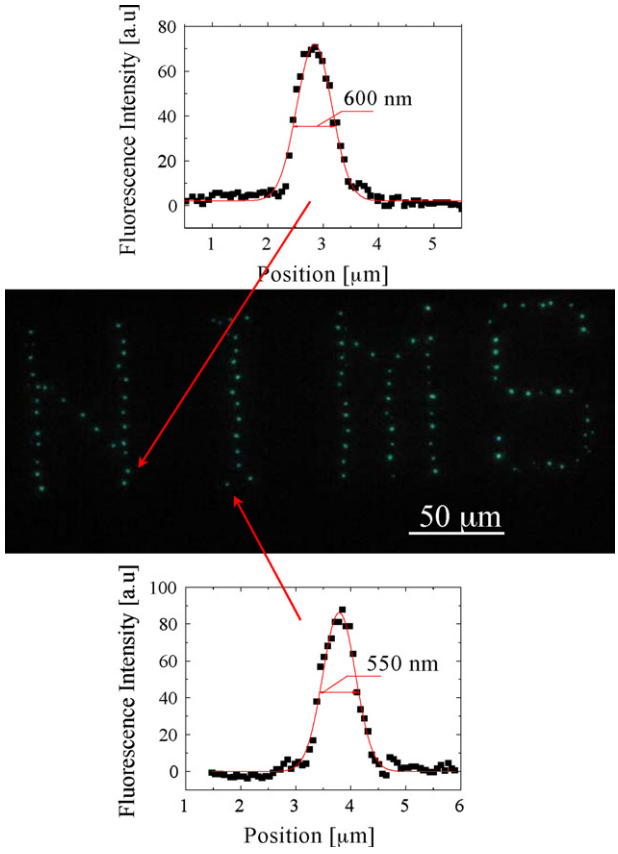

Fig. 9. Fluorescence micro-image of laser deposited C6 dots onto a stainless steel target (each dot was produced by a single laser pulse).

ductive material using a LIMMJ. Speaking of the overall credit of the method, it is necessary to add that it is a fast, inexpensive and reliable technique, which due to constant repeating results proves to be highly advantageous for practical use.

4. Conclusions

In this article, we have reported on a recent advanced method to modify the surface properties of various materials by means of a laser-induced molecular micro-jet and to prepare well-defined patterned surface with organic nano-molecular dots. We focused on the process of transferring organic matter from a source film to the target through a water layer, which helped us to implant ablated matter to the target without exposing it to decomposition and to reduce the size of an implanted or laser deposited dot. Due to the improvements in the laser implantation technique, we efficiently reduced the size of Coumarin 6 (C6) dots to the submicron scale. The smallest size of implanted or laser deposited organic dots was achieved on different targets, namely it was 2 μm on glass at laser fluence of 80 J/cm^2, 0.9 μm on ITO at 60 J/cm^2, 0.7 μm on copper at 2.3 J/cm^2 and 0.6 μm on stainless steel at 8.8 J/cm^2. Micro-Raman spectroscopy shows enhancements and shifts in the peaks of the C6 molecules due to chemical interactions between the copper target and the implanted molecules.

This new approach involved the transfer of the source matter to the target material through the gap filled with water. Thorough comparison of the C6 dots implanted through air and water demonstrated that laser water channelling has a crucial influence on the ablation mechanism of C6. Besides, we verified the ability of this new technique to implant various organic molecules through different types of liquid. The experimental results brought us to the conclusion that the size of the implantation area depends on laser fluence, the distance between the source and the target film, and fluid density.

Acknowledgements

The present work is supported by the Grant-in-Aid for Scientific Research (KAKENHI) in Priority Area "Molecular Nano Dynamics" from the Ministry of Education, Culture, Sports, Science and Technology. We would like to say special thanks to Horiba Company for the measurement of micro-Raman spectra. We are grateful to Prof. Jonathan Hobley for critical reading of the paper.

References

[1] H. Fukumura, Y. Kohji, K. Nagasava, H. Masahura, J. Am. Chem. Soc. 116 (1994) 10304.
[2] G. Gery, H. Fukumura, H. Masuhara, Chem. Commun. 7 (1998) 811.
[3] M. Goto, J. Hobley, T. Oishi, A. Kasahara, M. Tosa, K. Yoshihara, M. Kishimoto, H. Fukumura, Appl. Phys. A 79 (2004) 157.
[4] D.M. Karnakis, T. Lippert, N. Ichinose, S. Kawanishi, H. Fukumura, Appl. Surf. Sci. 127 (1998) 781.
[5] G. Gery, H. Fukumura, H. Masuhara, J. Phys. Chem. B 101 (19) (1997) 3698.
[6] H. Fukumura, H. Uji-I, H. Banjo, H. Masuhara, D. Karnakis, N. Ichinose, S. Kawanishi, K. Uchida, M. Irie, Appl. Surf. Sci. 127–129 (1998) 761.
[7] M. Goto, M. Kawanishi, H. Fukumura, Jpn. J. Appl. Phys. 38 (Part 2) (1999) L87.
[8] J. Hobley, M. Goto, M. Kishimoto, H. Fukumura, H. Uji-I, M. Irie, Mol. Cryst. Liq. Cryst. 345 (2000) 299.
[9] M. Kishimoto, J. Hobley, M. Goto, H. Fukumura, Adv. Mater. 13 (15) (2001) 1155.
[10] M. Goto, S. Kawanishi, H. Fukumura, Appl. Surf. Sci. 154–155 (2000) 701.
[11] M. Goto, V.L. Zhigiley, J. Hobley, M. Kishimoto, B. Garrison, H. Fukumura, J. Appl. Phys. 90 (9) (2001) 4755.
[12] Y. Pihosh, T. Oishi, M. Goto, A. Kasahara, M. Tosa, Appl. Surf. Sci. 241 (2005) 205.
[13] Y. Pihosh, M. Goto, A. Kasahara, M. Tosa, J. Photochem. Photobiol. A 183 (2006) 292.
[14] M. Goto, Y. Pihosh, A. Kasahara, M. Tosa, J. Appl. Phys. 45 (2006) L966.
[15] Y. Pihosh, M. Goto, A. Kasahara, M. Tosa, Thin Solid Films, (2007), doi:10.1016/j.tsf.2007.04.095.
[16] T. Vosgröne, A. Meixner, ChemPhysChem 6 (2005) 154.
[17] S. Nie, R.S. Emory, Science 275 (1997) 1102.
[18] N. Hayazawa, Y. Inouye, Z. Sekkat, S. Kawata, J. Phys. Chem. 117 (2002) 1296.
[19] Z. Tian, B. Ren, D.-Y. Wu, J. Phys. Chem. B 106 (2002) 9463.
[20] M. Moskovits, Rev. Mod. Phys. 57 (1985) 783.
[21] L. Berthe, A. Sollier, P. Peyre, R. Fabbro, E. Bartnicki, J. Phys. D: Appl. Phys. 33 (2000) 2142.
[22] J.R. Blake, M.C. Hooton, P.B. Robinson, R.P. Tong, Phil. Trans. R. Soc. Lond. A 355 (1997) 537.
[23] P. Prentice, A. Cuschierp, K. Dholakia, et al., Nat. Phys. 1 (2) (2005) 107.